10th World Congress on Structural and Multidisciplinary Optimization
May 19 - 24, 2013, Orlando, Florida, USA

Structural Optimization of Super-Repellent Surfaces

Andrea Cavalli, Peter Bøggild and Fridolin Okkels

Technical University of Denmark, Department of Micro- and Nanotechnology Ørsteds Plads Building 345 2800 Kgs. Lyngby
Corresponding author: acav@nanotech.dtu.dk

1. Abstract
Micro-patterning is an effective way to achieve surfaces with extreme liquid repellency. This technique does not rely on chemical coatings and is therefore a promising concept for application in food processing and bio-compatibile coatings. This super-repellent behaviour is obtained by suspending the liquid phase on a brush of micro- and nano-posts. In this way the contact with the substrate is minimized, and so is the adhesion force. While a lot of experimental work has been carried out in this field, relatively little has been done from a theoretical point in rationalizing and optimizing the geometry of the posts that generate the super-repellent effect. We here present two different approaches to obtain optimal liquid repellent surfaces, addressing some fundamental aspects of the problem. First, we focus on the wetting aspect, and we apply topology optimization to search for an optimal pattern to support the liquid phase in the suspended state [1]. Second, we consider simpler geometries, but we account for both the wetting and mechanical properties of the micro-posts, observing an interesting balance of conflicting design objectives [2]. In conclusion, we present a wide perspective on how numeric optimization tools can be applied to increase the understanding of this new, dynamic engineering field.

2. Keywords: Superhydrophobicity, Topology Optimization, Microfabrication, Multi-objective optimization.

3. Introduction
Several surfaces with extreme liquid repellent properties are found in Nature. Examples include plants [3], birds [4], insects [5] and arthropods [6]. In the last decades, several models [7, 8] have progressively shed light on the origin of such properties. As a matter of fact, micro- and nanometric textures are at the origin of the extreme liquid repellent properties observed on all these substrates. Recently, the advances in microfabrication have made it possible to realize artificial coatings that mimic such properties [9, 10, 11]. Artificial water- or oil-repellent surfaces have countless applications in medical, food and chemical industry. It is therefore of wide interest to understand and optimize this super-repellent property.

4. Wetting and textured surfaces

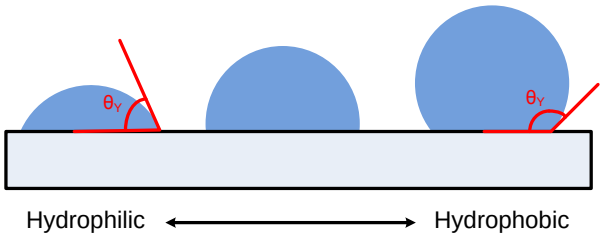

Figure 1: An hydrophilic surface (left side) favours the spreading of water and its adhesion to the substrate, while a hydrophobic surface (right side) favours almost spherical drops with little or no adhesion. The contact angle (shown in red lines) is a measure of these different behaviours.

The wetting behaviour of a liquid on a smooth solid surface can be described in terms of the contact angle θ_Y, i.e. the angle the liquid-air interface forms with the solid phase at the contact line (see Fig. 1). A small contact angle means it is energetically favourable for the liquid to wet the solid substrate,

therefore the adhesion will be strong. On the other hand, surfaces showing a large contact angle repel the liquid, which will form almost spherical droplets and easily detach from the surface. This parameter therefore captures the relevant chemical properties of the surface related to wetting.
The topography of the substrate, however, also play a relevant role.

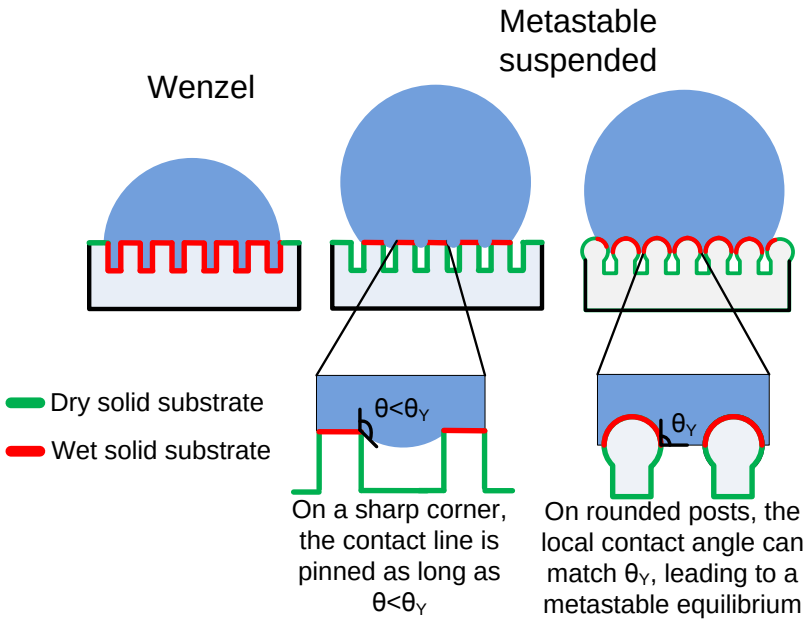

Figure 2: Sketch of the possible equilibrium positions for a droplet on a textured surface. The insertion shows a magnification of the idealised liquid-gas interface for the metastable configuration. Hydrophilic and slightly hydrophobic materials will favour the Wenzel configuration. However, the suspended configurations on the right side, which are associated with little adhesion to the substrate, can still be achieved as metastable states.

As it is possible to see in Fig.2, a drop on a textured surface can find different equilibrium states, depending on the interplay of geometrical and chemical properties. If the material is strongly hydrophilic, the presence of grooves or roughness will act like a "2D sponge", capturing the liquid by capillary imbibition (such a configuration is known as "Wenzel state", see Fig. 2). If, on the other hand, the material is strongly hydrophobic, the liquid will avoid contact with the substrate and will be suspended on the texture in a configuration called "fakir" or Cassie-Baxter state. The measured contact angle in this configuration is a weighted average involving the one with the solid substrate (θ_Y) and with air (180^o):

$$\cos\theta_{CB} = f_{sl}\cos\theta_Y - f_{gl}, \tag{1}$$

where f_{sl} represent the fraction of the drop base in contact with the solid phase, and f_{gl} is the fraction of the drop base in contact with air (for a smooth solid surface, $f_{sl} = 1$, $f_{gl} = 0$). Eq.1 shows how a suspended drop will always show a higher contact angle than the one expected on a smooth surface of the same material. This is qualitatively easy to understand, as the contact between the solid and liquid phase is reduced by the air pockets. As a matter of fact, while the suspended configuration is the equilibrium configuration only for highly hydrophobic materials, slightly hydrophobic and hydrophilic materials can also exhibit the Cassie configuration as a metastable configuration. This can happen in different ways, as sketched in the inserts of Fig.2. In one case, the contact line is pinned at the ridge of the posts, and unless a pressure is applied to deform the interface, the liquid will not move. On smooth posts, the local contact angle with the side wall can match θ_Y, which corresponds to a local energy minimum that prevents the interface from sliding further. If a pressure difference is applied across the liquid-air interface, it will deform. This will change the local angle between the interface and the solid wall, and could make it slide along the post sidewall, eventually losing the Cassie-Baxter configuration. If we want to assess the robustness of the Cassie-Baxter configuration for a given texture, we therefore need to characterize it with respect to deformations of the liquid-air interface. The mean curvature of the interface κ is related

to the pressure difference ΔP across it through the Young-Laplace relation:

$$\Delta P = \gamma \kappa, \tag{2}$$

where γ is the surface tension of the fluid, i.e. the energy cost per unit area of an interface between liquid and gas phases. Without going into mathematical details, Eq. 2 tells a lot about how much pressure a drop in the Cassie state can support before the liquid wets the substrate. For example, we see that a high surface tension γ means less interface deformation for the same applied pressure. Moreover, curvature has units of inverse length: this means that, the smaller the spacing in the texture, the harder it is to push the liquid among posts or grooves.

The concepts introduced in this section are all we need to understand the results presented in the following. In section 5, we apply topology optimization to find an optimal post cross section, that minimizes the interface deformation upon applied pressure, while keeping the solid fraction f_{sl} (and thus the apparent contact angle θ_{CB}) fixed. In section 6 we consider a similar problem (optimal support with limited surface covering), for overhanging structures, which are suitable for achieving the Cassie-Baxter state in hydrophilic materials. We therefore introduce the constraint of mechanical stability, which becomes relevant for the geometry we address.

5. Topology optimization of superhydrophobic surfaces

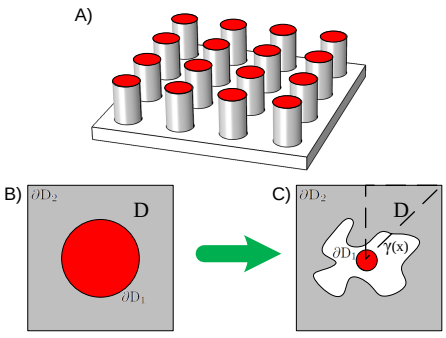

Figure 3: A) Sketch of the considered post array. B) Top view of a single post cell, for the basic circular cross section. C) Same view of a single cell, with a variable cross section (white area) around a fixed "nucleus" (red dot) . In the topology optimization procedure, the cross section is not fixed but varies according to the field $\gamma(\vec{x})$. The dashed line in C) shows the reduced computation domain that exploits the imposed symmetry of the cell. From [1].

As we described in the previous section, large displacements of the liquid-air interface could force a transition from the Cassie-Baxter to the Wenzel state, and thus a loss of the superhydrophobic properties of the pattern. The question we ask in this section is: for a given unit cell coverage f_{sl}, which post cross section provides the least interface displacement under a given applied pressure? As we will see, Topology Optimization is effective in answering this question. Our setup is sketched in Fig. 3A). We consider a typical square array of posts, which will provide the support to the interface. Instead of the typical circular post of Fig. 3B), we allow the cross section to change around a "solid" nucleus, according to a continuous design variable $\gamma(\vec{x})$ (3C). During the optimization steps, the design variable field $\gamma(\vec{x})$ is allowed to vary from 1 (completely solid region) to 0 (completely empty) through intermediate values, to account for different post shapes. The relevant physical variable in our simulations is the interface vertical displacement $S(\vec{x})$. If the interface bulges too much, the liquid will eventually touch the substrate among posts. The curvature of the interface upon applied pressure ΔP is given by the Young-Laplace equation 2, that can be formulated as a PDE (simulations units are used):

$$\begin{cases} \nabla \cdot \left(K(\gamma) \frac{\nabla S(\vec{x})}{|\nabla S(\vec{x})|} \right) = \Delta P & \text{on D} \\ S(\vec{x}) = 0 & \text{on } \partial \mathrm{D}_1 \\ \nabla S(\vec{x}) \cdot \vec{n} = 0 & \text{on } \partial \mathrm{D}_2. \end{cases} \tag{3}$$

The boundary conditions on ∂D_1 and ∂D_2 account for the central support and the periodicity of the unit cell, respectively. Eqs. 3 depend on the design variable $\gamma(\vec{x})$ through the function $K(\gamma)$ defined as:

$$K(\gamma) = 1 + \frac{(K_{max} - 1) \cdot q \cdot \gamma}{(q + 1 - \gamma)}. \tag{4}$$

This coupling was inspired by optimal heat conduction problems [12], and provides the desired interplay between the interface and the material distribution. Where $\gamma(\vec{x}) = 0$, $K(\gamma)$ is equal to 1, and we recover the Young-Laplace equation in absence of material. If $\gamma(\vec{x}) = 1$, $K(\gamma)$ is equal to K_{max} (set to 10^5 in our simulations). This corresponds to a huge local increase in the surface tension of the interface, which as a consequence will almost not deform, and we therefore get $\gamma(\vec{x}) = 1 \rightarrow S(\vec{x}) \simeq 0$ as the "solid phase" condition. The goal of the optimization procedure is to minimize the maximum interface deformation. A suitable choice for our objective function Φ will then be the squared integral displacement of the interface *

$$\Phi = \int_D S^2(\vec{x})\, dA. \tag{5}$$

The specific coupling between $\gamma(\vec{x})$ and $S(\vec{x})$ we choose leads to connected binary solid/empty designs, as $K(\gamma)$ "radiates" the support from ∂D_1 to the rest of the domain. We therefore do not allow the post to split into smaller isolated features. While the overall length scale of the texture is indeed a relevant parameter, we are here interested in the optimal shape of a *single* feature, which can then be scaled up or down according to the fabrication constraints.

At every optimization iteration, The Young-Laplace equation Eq. (2) is then solved to obtain $S(\vec{x})$. The objective function Φ and sensitivity $\frac{\delta\Phi}{\delta\gamma(\vec{x})}$ are then computed, and used to update $\gamma(\vec{x})$. Details on the sensitivity analysis and the implementation of the code can be found in the paper by Olesen et al. [14]. Eq.2 shows that the displacement of the interface is reduced for small length scales. This suggest that highly ramified design would probably be optimal, but difficult to fabricate on a micron or sub-micron length. In order to impose a minimum length scale, our optimization involves also a filtering step on the design variable $\gamma(\vec{x})$. At every iteration in the optimisation routine we calculate a smoothed version $\tilde{\gamma}(\vec{x})$ of the design variable $\gamma(\vec{x})$, applying a PDE filter [15]:

$$L_{diff}^2 \nabla^2 \tilde{\gamma}(\vec{x}) = \tilde{\gamma}(\vec{x}) - \gamma(\vec{x}). \tag{6}$$

$\tilde{\gamma}(\vec{x})$ is the quantity actually used in the objective function and sensitivity analysis. This process allows to control the minimum size of the features appearing in the optimal design and avoids optimal designs approaching the mesh length scale. The relevant PDEs are solved using the commercial software COMSOL, while the optimization relies on the method of moving asimptotes (MMA) [16].

Fig. 4 shows a typical sequence of steps in the topology optimization procedure. We start from an initial homogeneous distribution of material over the whole domain, equal to the desired solid surface coverage f_{sl}, which is imposed as a constraint. We observe a swift transition to a binary design, with the material accumulating along the diagonal of the unit cell. In later stages, further branching appears in the transverse direction. The overall result is quasi-fractal, with the clear objective of minimizing the gap between solid features. The optimal pattern is a planar analogue of several natural coatings, which employ hierarchical patterns on micro- and nano-roughness to achieve superhydrophobicity. As shown in Fig.5, the filter allows us to control the maximum resolution of the optimal design, in order to avoid mesh dependent effects and obtain feasible geometries.

Eventually, in Fig.6, we compare the interface displacement for a typical cylindrical post and a topology optimised one. As it is clear from Fig.6 B) and D), there is a significant reduction in the interface displacement. Another convenient feature of topology optimization is the possibility to adjust the optimal design to the symmetry of the unit cell. Similar results, for example, have been obtained for an hexagonal pattern.

*The most relevant quantity to determine the transition to the Wenzel state would actually be the angle between the post and the interface, which directly relates to the *maximum* displacement. As in mechanical structures optimizations, however, mean quantities are easier to evaluate and provide a smoother optimization. One could think of recovering the maximum displacement formulation by considering other means with increasingly high powers, $\Phi_\alpha = \sqrt[\alpha]{\int_D |S(\vec{x})|^\alpha \, dA}$.[13].

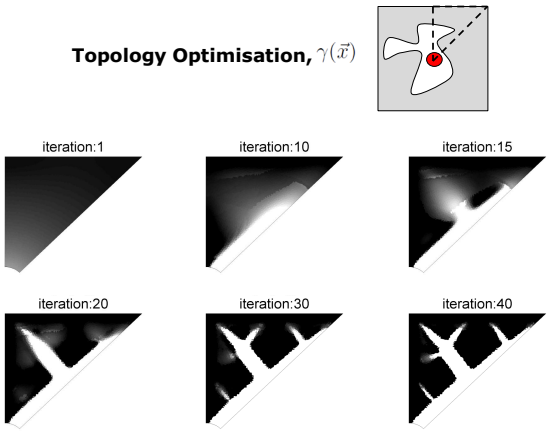

Figure 4: Snapshots of the topology optimization evolution, over a reduced domain that exploits the symmetry of the unit cell.

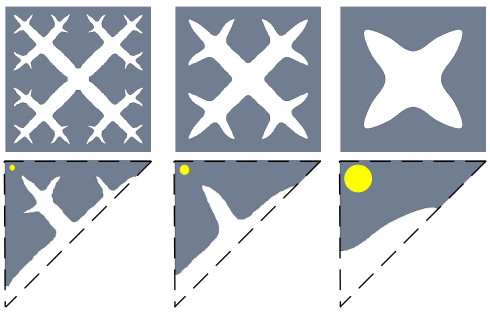

Figure 5: Optimal design for $f_{sl} = 0.3$ and L_{diff}=0.5, 1, 3 times the meshsize h_{mesh}. The radius of the yellow dot in each column is equal to L_{diff}. From [1].

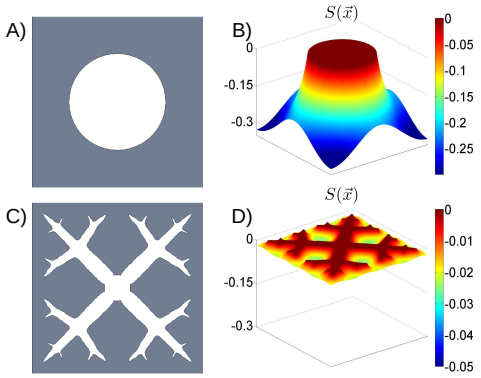

Figure 6: A) Top view of a cylindrical post with solid fraction $f_{sl} = 0.25$. B) Displacement plot for applied pressure $\Delta P = P_0$. C) Optimized material distribution with solid fraction $f_{sl} = 0.25$. D) Displacement plot for the topology optimized design. From [1].

6. Parametric optimization of inverse trapezoid olephobic surfaces

We will continue our analysis with a full three dimensional problem, involving a different geometry. The inverse trapezoid pattern presented by Im et al [11, 17] is an interesting example of how to obtain an hydrophobic behaviour from a hydrophilic material. Such surfaces are also known as oleophobic, since most materials are inherently oleophilic, and micro-patterning is almost the only way to make them oil-repellent. The undercut of this structures is meant to be complementary to the contact angle of the liquids, so that a local energy minimum is obtained and the drop remains suspended in a Cassie-Baxter state (see inset in Fig.2). These posts can be fabricated with high precision at a characteristic size of $L_0 = 5\ \mu m$ in cross-linked PDMS, using backside diffuse lithography. In Fig.7a) we show the relevant

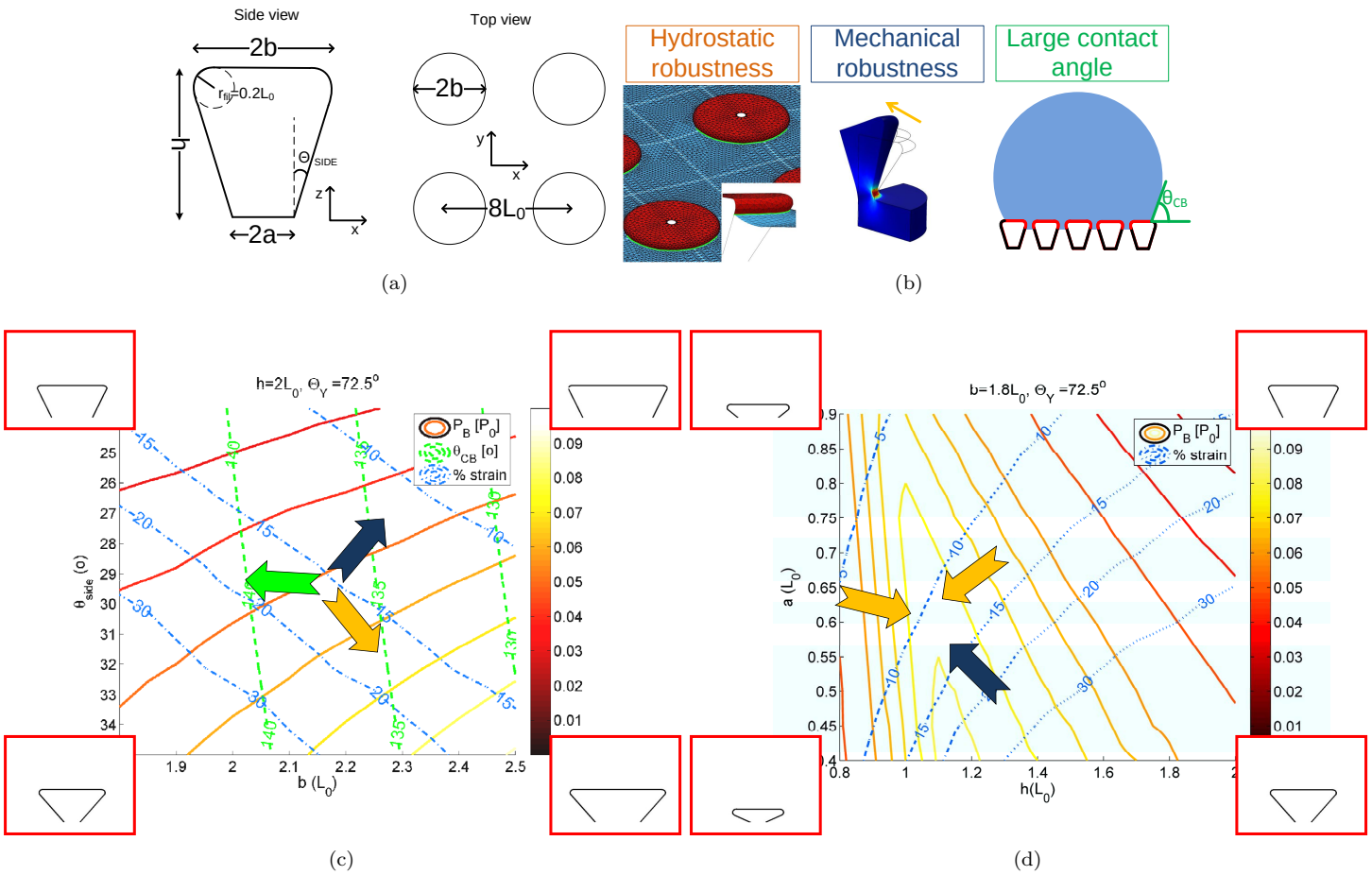

Figure 7: (a):Relevant geometric parameters to characterize the inverse trapezoid array. (b): optimization objectives for a robust oleophobic surface. c): optimization objectives in the b-θ_{side} parameter space (h=$2L_0$), $\cos\theta_Y = 0.3$. d): optimization objectives in the a-h parameter space (b=$1.8L_0$), $\cos\theta_Y = 0.3$. In c)-d), the color legend is as follows: warm color scale: Breakthrough pressure, Green: apparent contact angle θ_{CB} , Blue: maximum percent strain. Each arrow represent an optimality direction, for mechanical robustness (blue), apparent contact angle (green) and maximum breakthrough pressure (orange). In each corner of the geometric space, the corresponding trapezoid is shown. Adapted from [2].

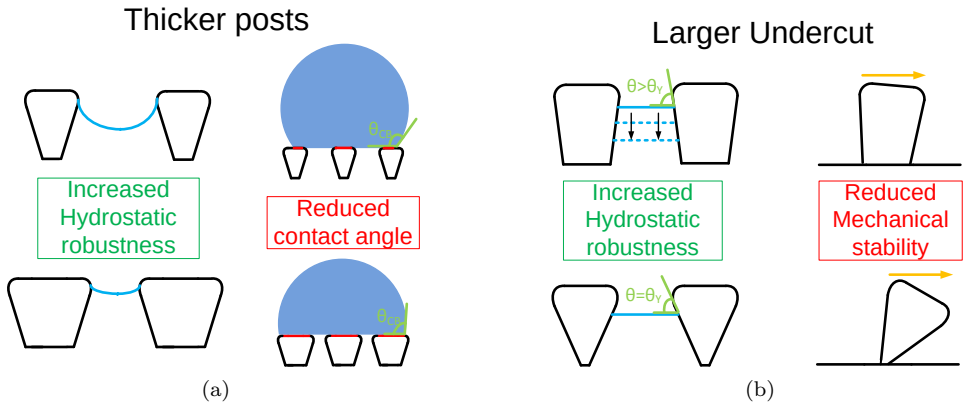

Figure 8: (a): Relevant geometric parameters characterizing the inverse trapezoid geometry. (b): Optimization objectives for a robust oleophobic surface.

parameters that describe our geometry: the post height h, top radius b, base radius a and side angle $\theta_{side} = \frac{b-a}{h}$ †. In Fig. 7b) we show the relevant optimality criteria for a robust oleophobic surface: A large contact angle θ_{CB}, a Cassie-Baxter state resistant to pressures up to P_B and a mechanically robust geometry. Combining mechanical and wetting properties is the main point of this analysis, since an oleophobic surface is expected to be able to support different kind of wear and stresses in everyday applications. We consider a simple load, i.e. a uniform shear stress on the top of the post. We then use linear elasticity to evaluate the maximum principal strain in the structure, which gives a qualitative measure of the robustness of the posts. As expected, the largest stresses and strains are found at the neck of the pillar, and depend significantly on the post geometry. It is easy to see how these optimization objectives will be conflicting. For example, if we increase the top radius a while keeping the unit cell size and all the others parameters fixed, we effectively reduce the distance between posts. This increases the stability of the Cassie-Baxter configuration, but reduces the apparent angle θ_{CB}, since the wetted solid fraction f_{sl} per unit cell also increases (as sketched in Fig.8a)). Similarly, increasing the trapezoids undercut will allow a more robust Cassie Baxter state, since a wider range of contact angles can be accommodated on the post sidewalls. However, the narrow base of the posts will suffer high stresses upon a shear load, which might result in a mechanical failure of the structure (as sketched in Fig.8b)). If we combine all these objectives together, we can then find a localized optimum in the design parameter space, i.e. a reliable suspended state for a given contact angle and mechanical performance. In Figs. 7c) and 7d) we plot contour lines for the contact angle θ_{CB} (green dotted lines), the maximum strain (blue dashed lines) and the maximum sustainable pressure P_B (warm colour lines) in the $b - \theta_{side}$ and $a - h$ parameter spaces. Relevant post geometries are also shown in the corners. It is apparent how the different optimization goals act against each other, so that a nontrivial optimum can be found according to performance specifications. The breakthrough pressure in Fig.7c) and 7d) where obtained using the interface simulator Surface Evolver [19]. The post strain was calculated with COMSOL.

8. Conclusions and outlook

In this paper we described two different aspects of optimal liquid repellency, considering different objective functions. First we applied topology optimization to superhydrophobic surfaces, in order to maximise the robustness of the non-wetting configuration. We then considered inverse trapezoid posts, which are able to suspend low surface tension fluids, and looked for an optimal shape which accounted for both wetting and mechanical properties. We conclude that wetting phenomena involve several physical properties, which can easily increase the modelling and computational effort. It is therefore fundamental to identify suitable parameters and objectives, which can provide a simple yet quantitative description of the superhydrophobic behaviour. Ongoing work regards the fabrication and characterization of the discussed patterns, as well as applying this approach to other wetting behaviours, such as directional liquid motion or spreading.

9. Acknowledgements

The authors thank P.A. Fisker fonden for sponsoring the participation to this conference.

10. References

[1] Andrea Cavalli, Peter Bøggild, and Fridolin Okkels. Topology optimization of robust superhydrophobic surfaces. *Soft Matter*, 9(7):2234–2238, 2013.

[2] A. Cavalli, P. Boggild, and F. Okkels. Parametric optimization of inverse trapezoid oleophobic surfaces. *Langmuir*, 2012.

[3] C Neinhuis and W Barthlott. Characterization and distribution of water-repellent, self-cleaning plant surfaces. *Annals of Botany*, 79(6):667–677, 1997.

[4] E. Bormashenko, Y. Bormashenko, T. Stein, G. Whyman, and E. Bormashenko. Why do pigeon feathers repel water? hydrophobicity of pennae, cassie–baxter wetting hypothesis and cassie–wenzel capillarity-induced wetting transition. *Journal of colloid and interface science*, 311(1):212–216, 2007.

†The overall length scale L_0 of the features will also play a relevant role [18]. Indeed, scaling down the array would provide better support at the liquid-air interface while not affecting the contact angle. However, the resolution of the lithographic technique is finite, and defects will likely be more frequent on smaller features. In our modelling we therefore do not change the length scale of the system, but rather focus on the posts' shape and aspect ratio, which could then be scaled down to the smallest feasible size.

[5] Xuefeng Gao and Lei Jiang. Biophysics: water-repellent legs of water striders. *Nature*, 432(7013):36–36, 2004.

[6] Ralf Helbig, Julia Nickerl, Christoph Neinhuis, and Carsten Werner. Smart skin patterns protect springtails. *PloS one*, 6(9):e25105, 2011.

[7] Robert N Wenzel. Resistance of solid surfaces to wetting by water. *Ind. Eng. Chem*, 28(8):988–994, 1936.

[8] A. B. D. Cassie and S. Baxter. Wettability of porous surfaces. *Trans. Faraday Soc.*, 40(0):546–551, 1944.

[9] A. Tuteja, W. Choi, J. M. Mabry, G. H. McKinley, and R. E. Cohen. Robust omniphobic surfaces. *Proceedings of the National Academy of Sciences*, 105(47):18200, 2008.

[10] J. Bico, C. Marzolin, and D. Quéré. Pearl drops. *EPL (Europhysics Letters)*, 47:220, 1999.

[11] Maesoon Im, Hown Im, Joo-Hyung Lee, Jun-Bo Yoon, and Yang-Kyu Choi. A robust superhydrophobic and superoleophobic surface with inverse-trapezoidal microstructures on a large transparent flexible substrate. *Soft Matter*, 6(7):1401–1404, 2010.

[12] A. Gersborg-Hansen, M. P. Bendsøe, and O. Sigmund. Topology optimization of heat conduction problems using the finite volume method. *Structural and multidisciplinary optimization*, 31(4):251–259, 2006.

[13] M. P. Bendsøe and O. Sigmund. *Topology optimization: theory, methods, and applications*. Springer Verlag, 2003.

[14] L. H. Olesen, F. Okkels, and H. Bruus. A high-level programming-language implementation of topology optimization applied to steady-state navier–stokes flow. *International Journal for Numerical Methods in Engineering*, 65(7):975–1001, 2006.

[15] B. S. Lazarov and O. Sigmund. Filters in topology optimization based on helmholtz-type differential equations. *International Journal for Numerical Methods in Engineering*, 86(6):765–781, 2011.

[16] K. Svanberg. The method of moving asymptotes: a new method for structural optimization. *International journal for numerical methods in engineering*, 24(2):359–373, 1987.

[17] Maesoon Im, Hwon Im, Joo-Hyung Lee, Jun-Bo Yoon, Yang-Kyu Choi, et al. Analytical modeling and thermodynamic analysis of robust superhydrophobic surfaces with inverse-trapezoidal microstructures. *Langmuir*, 26(22):17389, 2010.

[18] Shreerang S Chhatre, Wonjae Choi, Anish Tuteja, Kyoo-Chul Park, Joseph M Mabry, Gareth H McKinley, and Robert E Cohen. Scale dependence of omniphobic mesh surfaces. *Langmuir*, 26(6):4027–4035, 2009.

[19] Kenneth A Brakke. The surface evolver. *Experimental mathematics*, 1(2):141–165, 1992.